Journal of Computational Electronics 1: 317–321, 2002

Atomistic Electronic Structure Calculations of Unstrained Alloyed Systems Consisting of a Million Atoms

FABIANO OYAFUSO,* GERHARD KLIMECK AND R. CHRIS BOWEN
Jet Propulsion Laboratory, California Institute of Technology, Pasadena, CA 91109, USA
fabiano@jpl.nasa.gov

TIMOTHY B. BOYKIN
Department of Electrical and Computer Engineering and LICOS, University of Alabama in Huntsville, Huntsville, AL 35899, USA

Abstract. The broadening of the conduction and valence band edges due to compositional disorder in alloyed materials of finite extent is studied using an sp^3s^* tight binding model. Two sources of broadening due to configuration and concentration disorder are identified. The concentrational disorder dominates for systems up to at least one million atoms and depends on problem size through an inverse square root law. Significant differences (over 12 meV) in band edge energies are seen depending on choice of granularity of alloy clusters.

Keywords: alloys, disorder, tight-binding, bandstructure, NEMO

1. Introduction

As device sizes shrink, the relative importance of nanoscale features owing to the granularity of matter increases. Non-atomistic models such as $\mathbf{k} \cdot \mathbf{p}$, which assume a "jellium"-like representation of matter, can no longer accurately characterize the electronic structures of systems in which effects arising from interfaces and disorder are important (Fu, Lin-Wang and Zunger 1998). Instead, atomistic models such as tight-binding or pseudopotentials must be employed. Useful implementations of such models are semi-empirical in nature and require a larger set of parameters than that which is utilized by $\mathbf{k} \cdot \mathbf{p}$. A first step in the critical path toward nanostructure simulation is a proper characterization of the bulk properties of alloys. This paper describes simulation results obtained using the tight-binding-based nanostructure simulator NEMO-3D for bulk alloyed systems and convergence issues arising from the random distribution of cations in unstrained ternary III–V systems.

*To whom correspondence should be addressed.

NEMO-3D, an extension to three dimensions of the NEMO-1D device simulator developed at Raytheon/TI (Bowen *et al.* 1997), has been developed to model quantum dot structures on high performance commodity clusters (Beowulfs). A detailed description of NEMO-3D can be found elsewhere (Klimeck to appear). NEMO-3D is based on a nearest-neighbor tight-binding model that typically employs a 20 orbital $sp^3d^5s^*$ basis associated with each atomic lattice site. Faster simulations are possible using a restricted 10 orbital sp^3s^* or a single band (single s) orbital basis. The coupling energies between these orbitals can be computed by using a genetic algorithm package (Klimeck *et al.* 2000a, b) to determine a best fit to experimentally measurable bulk properties such as bandgaps, effective masses and strain-induced shifts.

A realistic atomic simulation is computationally taxing. For example, the modeling of a horizontal array of four self-assembled InAs quantum dots of 30 nm diameter and 5 nm height embedded in GaAs of buffer width 5 nm and separated by 20 nm requires a simulation domain encompassing 5.2 million atoms. Electronic structure calculations on such a system entails

diagonalization of a sparse Hamiltonian of order $\sim 10^8$, whose large size necessitates computation on large parallel computers. NEMO-3D has been developed to minimize communication costs and memory usage such that each processor holds information relevant only to the set of atoms associated with that processor. Compact data structures utilizing Hamiltonian symmetries enable simulations of up to 15 million atoms on a 64 processor system with 1 GB/processor.

2. Simulation

One important capability of an atomistic model is the capability to incorporate disorder realistically. Two categories are typically identified (Chen and Sher 1995) in alloys: positional disorder, arising from deviations in the atomic equilibrium positions due to strain, and compositional disorder, arising from the distribution of different cation-anion bonds throughout the alloy. In this paper we restrict ourselves to study only compositional disorder and therefore study $Al_xGa_{1-x}As$, whose constituents AlAs and GaAs have essentially identical bond lengths. No strain effects need to be considered here. In this work we use the 10 band sp^3s^* model where the parameters for GaAs and AlAs are given in Table 1.

A supercell consisting of a number of primitive cells is selected containing a random distribution of Ga and Al cations. Periodic boundary conditions on the supercell are applied such that translations equal to a primitive direct lattice vector $\mathbf{R}$ of the supercell induce shifts of $e^{i\mathbf{k}\cdot\mathbf{R}}$ according to Bloch's theorem. The resulting supercell Hamiltonian $\mathcal{H}$ is then diagonalized. Although $\mathbf{k}$ is in a strict sense no longer a good quantum number, since translational invariance on the scale of the primitive cell no longer applies, one can still obtain fundamental band gaps from this approach by diagonalizing $\mathcal{H}(\mathbf{k} = 0)$. As the supercell size increases, the variation in energy gap for different random configurations tends to zero. Figure 1(a) compares the energy gap determined from using a sufficiently large supercell with experiment (Landolt-Bornstein 1982) and with the virtual crystal approximation (VCA). Good agreement between the alloy result and experiment below the $\Gamma - X$ crossover point is demonstrated. Note, however, that the VCA result in which the orbital coupling potentials are linearly interpolated between GaAs and AlAs prior to diagonalization shows marked disagreement with experiment. This result underscores the fact that the order in which the averaging and the diagonalization is performed can lead to drastically different results on the order of 100 meV.

There are two sources of compositional disorder. One source is configurational and arises from the distribution of different cations throughout the alloy *subject to the constraint of a fixed concentration*. The other source is concentrational and stems from the fact that a growth process will never produce nanostructures with identical concentrations each time. NEMO 3-D currently supports two compositional disorder models. The first makes the simplifying assumption that neighboring cations are completely uncorrelated so that the species at a particular cation site is determined randomly according to the expected concentration x and independently of the configuration of the remainder of

Table 1. Bandstructure parameters (eV).

Parameter	GaAs	AlAs
$E(s,a)$	−8.510704	−7.738226
$E(p,a)$	0.954046	0.872374
$E(s,c)$	−2.774754	−1.101736
$E(p,c)$	3.434046	3.475774
$E(s^*,a)$	8.454046	7.373508
$E(s^*,c)$	6.584046	6.615774
$V(s,s)$	−6.451300	−6.664200
$V(x,x)$	1.954600	1.878000
$V(x,y)$	4.770000	3.860000
$V(sa,pc)$	4.680000	5.600000
$V(sc,pa)$	7.700000	6.800000
$V(s^*a,pc)$	4.850000	4.220000
$V(pa,s^*c)$	7.010000	7.300000
Δ_a	0.420000	0.420000
Δ_c	0.174000	0.024000
Γ_8^V offset	0	−0.545148

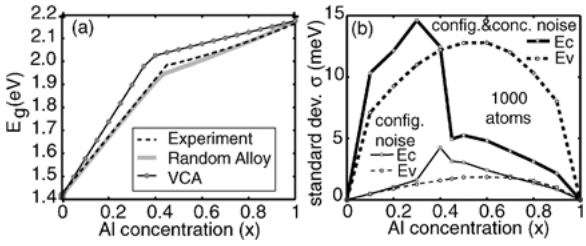

Figure 1. (a) Comparison of random alloy bandgaps and VCA result with experiment (Landolt-Bornstein 1982). (b) Fluctuations in band edges for a small system of roughly 1000 atoms with (dashed curve) and without (solid curve) concentrational broadening.

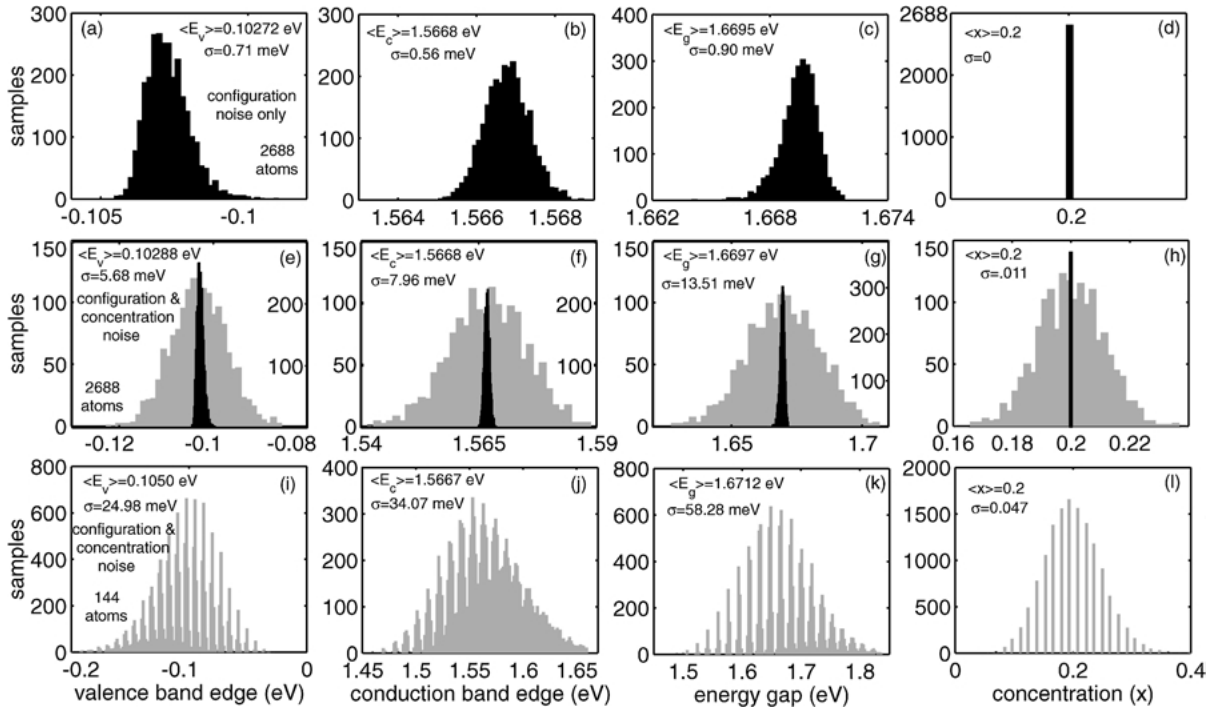

Figure 2. Columns from left to right show valence band edge, conduction band edge, energy gap, and concentration. First two rows are for a 3000 atom system including configurational disorder only (a–d) and total compositional broadening (e–h). Third row shows total broadening for a small system of 144 atoms.

the supercell. Within this model the cation concentrations can be allowed to vary statistically or they can be pinned to a single value, enabling the simulation of pure configuration noise. The second model of compositional disorder increases the granularity of the disorder from the atomic level to that of the cubic cell, so that all four cations within a unit cell are of the same species.

Figure 1(b) compares the standard deviation of band edge energies for a small system consisting of only 1000 atoms. For this small system, the broadening due to compositional disorder is large (as much as 12 meV) and dominates over the purely configurational disorder. Note that unlike the valence band edge which varies smoothly with Al concentration, the broadening of the conduction band edge varies sharply near the direct/indirect transition point at $x \approx 0.45$. The reason for this abrupt transition is a strong correlation between the concentration disorder and the band edge (shown further below). Variations in the band edge energy are related linearly to the variations in concentration ($\Delta E \propto \frac{dE}{dx}\Delta x$). Since there is a change in slope in the conduction band edge $\frac{dE_c}{dx}$ at $x \approx 0.45$ there will be a change in the variation ΔE_c. There are no features in the valence band distributions, since the valence band edge varies smoothly as a function of x.

Figure 2 shows the statistical distribution of the conduction band edge, valence band edge, energy gap, and concentration of a random ensemble of supercells. The histograms on the first row correspond to a system of approximately 3000 atoms whose concentration is pinned to 20% Al. At this size the standard deviations are under 1 meV for both the conduction band edge and valence band edge. Notice that while the distribution of the electronic spectrum is symmetric, the hole spectrum is asymmetrically skewed toward the bandgap. This skew in the valence band edge is evident even in larger system consisting of up to one million atoms. At present we suspect that the skewing is induced by the valence band degeneracy at the valence band edge, since we have found a similar skewing of the conduction band edge near the $\Gamma - X$ crossover point. The hole energy asymmetry is also evident in the band gap distribution.

The second row in Fig. 2 illustrates the effect of the introduction of concentration noise compared to the energy scaled distributions of the first row. All distributions appear to be Gaussian with much larger standard

deviations ($\sigma_{Ec} = 5.68$ meV and $\sigma_{Ev} = 7.96$ meV). No asymmetry is evident compared to pure configurational broadening. The last row of Fig. 2 shows the distribution of a very small system consisting of 144 atoms and offers another interpretation of the total compositional broadening. Because of the small size of this system, the set of allowed concentrations is descrete, and the occupation of the allowed concentrations follows a Gaussian as seen in Fig. 2(1). Thus, the total broadening consists of the superposition of the configurational broadening around each allowed concentration.

Figure 2 also shows that the standard deviations of the conduction and valence band edges add up to the broadening of the band gap for the case of compositional broadening but not for the case of configurational broadening. The strong correlation in the case of compositional broadening between E_c and E_v is depicted in Fig. 3(b) by the narrow distribution of scatter points. This result is reasonable, since the broadening arises from variations in the overall concentration and since the conduction and valence bands both move in such a way as to increase the energy gap as the concentration increases. No such correlation is visible in Fig. 3(a). Figure 3(c) shows a combination of (a) and (b) where little correlation is evident within a given discrete concentration, but significant correlation exists as the concentration varies. A plot of E_c vs. x (not shown here) translates the strong correlation between E_c and E_v shown in Fig. 3(b) to a linear relationship between E_c and x. This linear relation leads to the cusp in $\Delta E_c(x)$ shown in Fig. 1(b) at the change of slope of $E_c(x)$ at $x \approx 0.45$ shown in Fig. 1(a).

Figure 4 examines the dependence of the different noise sources on the atom number, N, in the supercell. In Fig. 4(a) and (b), only configurational broadening is considered and two regions of interest are evident. For $N < 1000$, the means of E_c and E_v tend in such a way

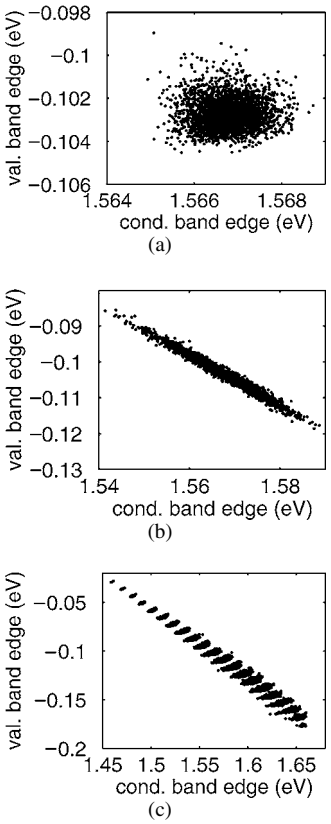

Figure 3. Scatter plots of E_v vs. E_c of the samples shown in the distributions in the first two columns of Fig. 2. (a) The pure configuration disorder shows hardly any correlation between E_c and E_v (circular distribution). (b) The concentration disorder shows a strong correlation as indicated by the straight line. (c) The small system shows clearly the correlation within small clusters.

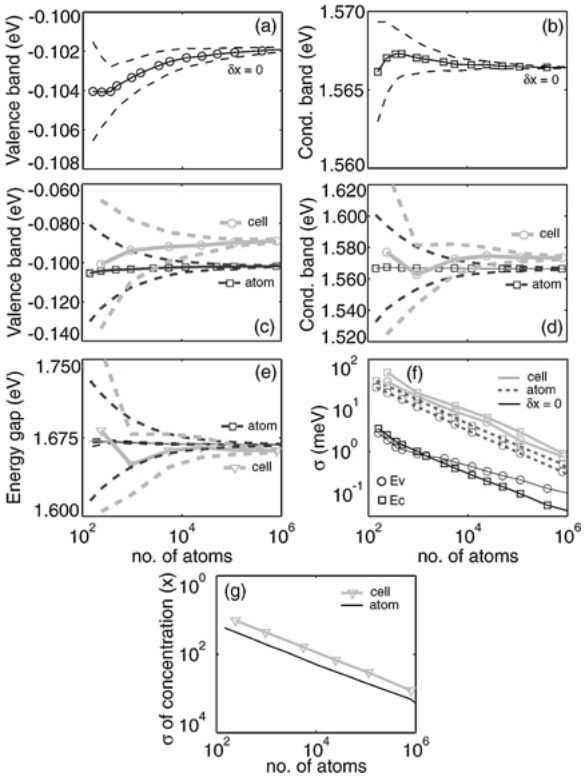

Figure 4. (a–d) Means of valence and conduction band edges (solid) with associated standard deviation (dashed) for configurational broadening (black) and total compositional broadening with atomic (dark gray) and cellular (thick light gray) granularity. Energy gap (e) and standard deviation (f) for the three broadening cases. Standard deviation of concentration (g) has a $N^{-1/2}$ dependence.

as to decrease the band gap as N decreases. For $N > 1000$, the trend is reversed with a slow convergence to the $N = \infty$ value.

Although the degree of correlation among neighboring cations is not a fully resolved matter, there is theoretical evidence for the existence of some short-range ordering in alloys (Chen and Sher 1995). Figure 4(c–e) demonstrate that clustering on a cellular level can produce band edges that differ significantly from alloys in which the granularity of randomness is on the atomic level. Here E_v and E_c are raised by 12.8 meV, 6.7 meV, respectively, resulting in an overall bandgap decrease of 5.9 meV.

Finally Fig. 4(f) demonstrates the decrease in standard deviation with system size. Both simulations which include the compositional disorder very closely follow a $\sigma = N^{-1/2}$ power law, since the standard deviation of the concentration also follows this law (shown in Fig. 4(g)). The variation in the alloy energy gap with only configurational disorder remains at least an order of magnitude smaller than with the full disorder, and as in the case of the convergence of the mean, there is a discontinuity in slope at $N = 1000$.

3. Conclusion

A numerical study of disordered alloys has been presented. Two principal components of the compositional disorder have been identified, the most dominant of which is the due to the overall variation in concentration. Finally, clustering in alloys has been shown to vary band edges in excess of 12 meV.

Acknowledgments

The work described in this publication was carried out at the Jet Propulsion Laboratory, California Institute of Technology. The Beowulf cluster on which our calculations were performed was provided by funding from the NASA Offices of Earth Science, Aeronautics, and Space Science.

References

Bowen R.C., Klimeck G., Lake R.K., Frensley W.R., and Moise T. 1997. J. Appl. Phys. 81: 3207.

Chen A.-B. and Sher A. 1995. Semiconductor Alloys, Plenum Press, New York.

Fu H., Lin-Wang, and Zunger A. 1998. Phys. Rev. B 57: 9971.

Klimeck G. Computer Modeling in Engineering and Science, accepted for publication, in print, 2002.

Klimeck G., Bowen R.C., Boykin T.B., Salazar-Lazaro C., Cwik T.A., and Stoica A. 2000a. Superl. and Microstr. 27(2): 77–88.

Klimeck G., Bowen R.C., Boykin T.B., and Cwik T. A. 2000b. Superl. and Microstr. 27(5/6): 519–524.

Landolt-Bornstein L. 1982. Numerical Data and Functions in Science and Technology, Vol. 22a. Springer, Berlin.